

See discussions, stats, and author profiles for this publication at: <https://www.researchgate.net/publication/49712437>

Atoms and Bonds in Molecules from Radial Densities

ARTICLE *in* THE JOURNAL OF PHYSICAL CHEMISTRY A · FEBRUARY 2011

Impact Factor: 2.69 · DOI: 10.1021/jp1093417 · Source: PubMed

CITATIONS

2

READS

34

3 AUTHORS:



Peter L Warburton

Memorial University of Newfoundland

22 PUBLICATIONS 204 CITATIONS

[SEE PROFILE](#)



Raymond A Poirier

Memorial University of Newfoundland

140 PUBLICATIONS 2,007 CITATIONS

[SEE PROFILE](#)



Devin Nippard

Memorial University of Newfoundland

2 PUBLICATIONS 3 CITATIONS

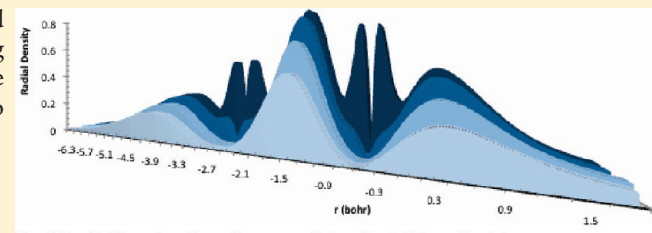
[SEE PROFILE](#)

Atoms and Bonds in Molecules from Radial Densities

Peter L. Warburton,* Raymond A. Poirier,* and Devin Nippard

Department of Chemistry, Memorial University, St. John's, NL A1B 3X7, Canada

ABSTRACT: Radial densities are explored as an alternative method for partitioning the molecular density into atomic regions and bonding regions. The radial densities for atoms in molecules are similar to those of an isolated atom. The method may also provide an alternative to Bragg—Slater radii.



Total Radial Density along lines parallel to the CO bond in CO.

INTRODUCTION

The definition of atoms in molecules (AIM) has been of interest to chemists for decades.^{1–7} The main motivations for defining AIM are linked to the chemist's concept of functional groups; similar chemistry implies similarity of the atoms involved, regardless of the differences in the functional group's molecular environment. Therefore, molecular properties are conceivably better understood via additivity of AIM atomic properties, and the effect of differing environments on AIM can be analyzed via comparisons of atomic properties. Such comparisons are usually based on the AIM electron density but comparisons of many other atomic properties are possible. Furthermore, predicting molecular properties for molecules of computationally intractable size can be accomplished by assuming transferability of the AIM atomic properties, and the building of larger molecules from appropriate AIM representations.

However, the definition of AIM is still a contentious issue. Bader's quantum theory of atoms in molecules (QTAIM)^{2,8,9} defines the AIM via the determination of zero flux surfaces where the gradient of electron density is zero for all points on the surface. As such, Bader asserts that "real atoms do not overlap" and that an "overlapped atom is unavoidably contaminated by its neighbors."⁹

Other approaches to AIM rely on the notion that atoms do overlap, and attempt to resolve atomic properties by partitioning the molecular electron density into overlapping individual atomic densities. However, much like population analysis,¹⁰ such partitioning can be arbitrarily accomplished via many differing methods, leading to different overlapping spherical^{6,7,11} fuzzy electron densities of AIM.

Stewart^{3,12} introduced the idea of describing the spherical atomic densities of AIM in terms of electron population analysis of X-ray diffraction data using least-squares projection methods onto atomic density functions. Further refinements form approximations dubbed Stewart—Slater atoms, which yield AIM "that are intuitively plausible and chemically

Table 1. Bragg—Slater Radii (BSR) (bohr) Used To Determine the Becke Weights

atom	radius
H ^a	0.66
Li	2.74
Be	1.98
B	1.61
C	1.32
O	1.13
F	0.94
Mg	2.83
Cl	1.89
K	4.16
Ca	3.40

^a The Bragg—Slater radius of H is 0.47.

useful."¹¹ Further explorations of this concept led to connections between Stewart densities and Coulomb energies¹³ and improved methods of generating Stewart atoms.^{14,15} Noted drawbacks of these Stewart atoms include regions of negative atomic density and oscillations at large distances from the nuclei that complicate the fitting of Stewart atoms by a finite radial basis set.¹⁵

Hirshfeld⁴ proposed defining AIM based on dividing the molecular electron density into atomic components by using a stockholder approach. A promolecule is created by addition of noninteracting free atomic densities centered at nuclear positions of the molecule of interest. Partitioning of the actual molecular density at each point is accomplished by using the relative contribution of free atomic densities in the promolecular density at the same point. However, Davidson¹⁶ and Bultinck⁶ noted problems with this approach. First, Hirshfeld

Received: September 29, 2010

Revised: December 7, 2010

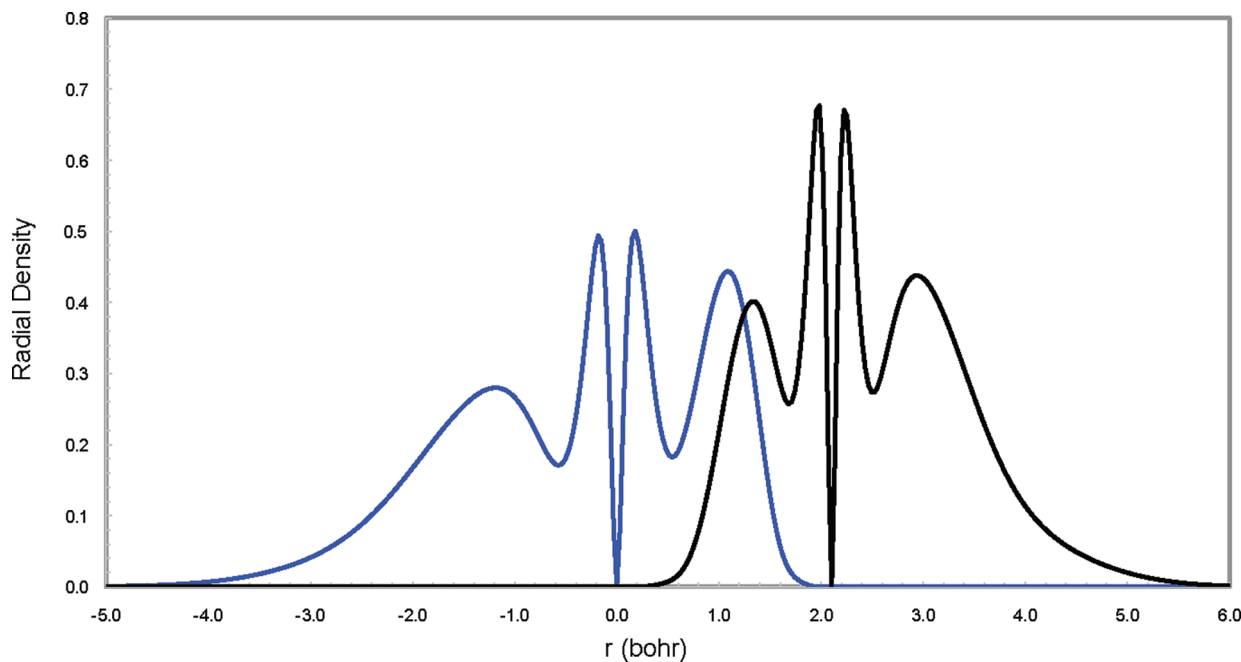


Figure 1. Radial densities for C (0.0) and O (2.105) along the CO bond in CO.

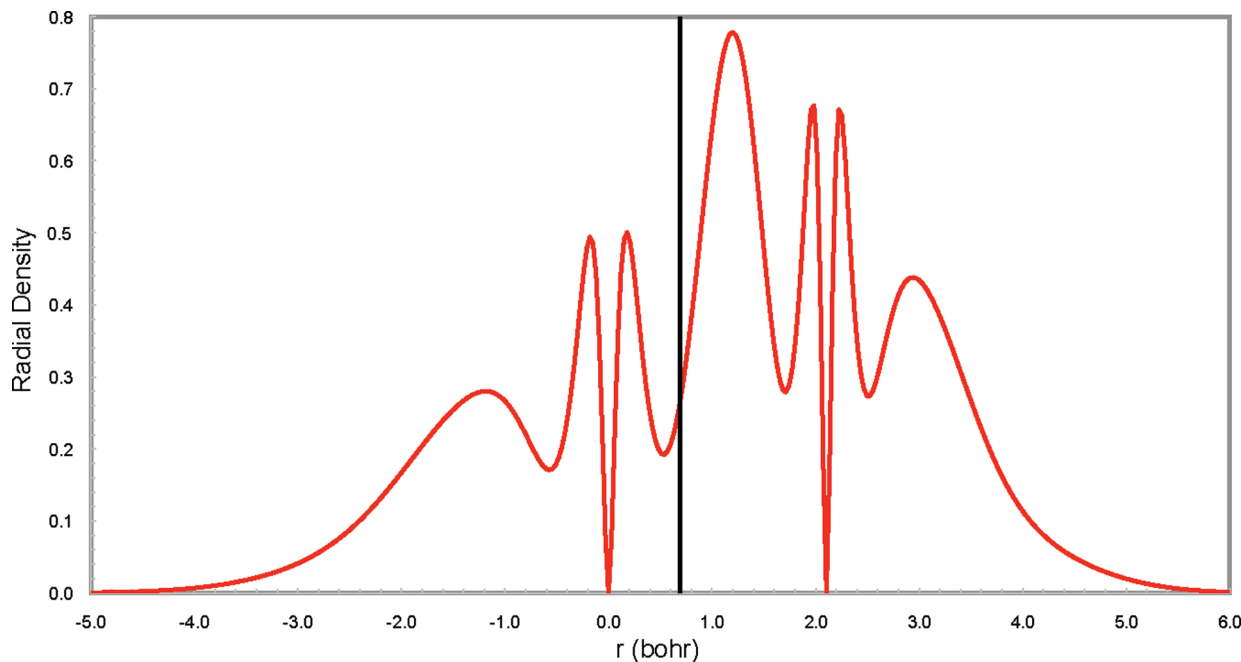


Figure 2. Total radial density along the CO bond in CO. The solid line corresponds to the bond critical point.

atomic charges tend to be almost zero since the approach tries to make the AIM as similar as possible to the free atom in the promolecule. Also, Hirshfeld atoms do depend on the choice of free atoms used to make the promolecule. One can use either neutral atoms or ions as the free atomic representations, and different choices can lead to different Hirshfeld atoms for the same molecule.

Bultinck's response to these problems was to create an iterative procedure where Hirshfeld AIM are generated and then used to create renormalized free atomic densities, which are used to create the next promolecule. The process is

iterated until no net charge transfer occurs and spherical atomic densities can be obtained through use of the atom condensed Fukui function. These Hirshfeld-I AIM have larger net charges and no longer show a dependence on the original promolecule choice. The Hirshfeld-I AIM uniqueness was further investigated¹⁷ and Hirshfeld-I charges were studied in terms of molecular electrostatic potentials, giving reasonable dipole moments from the monopole level.¹⁸

A different iterative stockholder approach has been presented by Wheatley.⁷ These iterative stockholder atoms (ISA) do not rely on a promolecule choice but rather start with arbitrarily

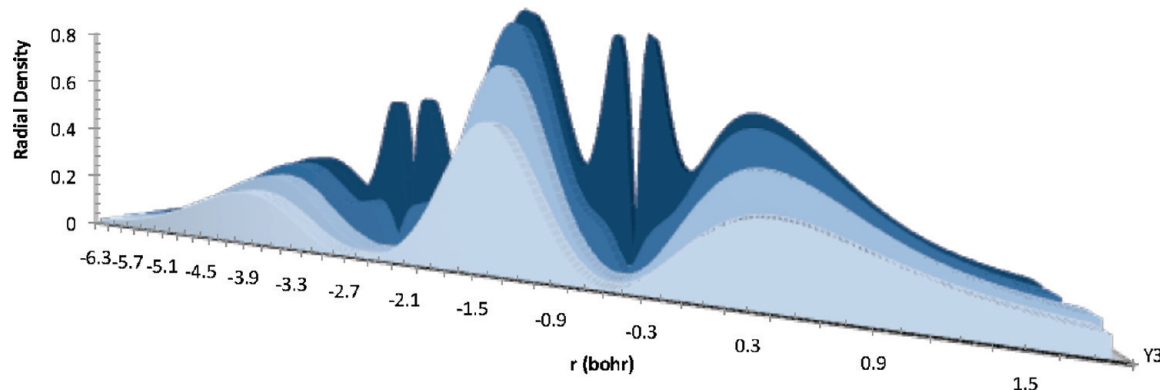


Figure 3. Total radial density along lines parallel to the CO bond in CO. Each line is offset by 0.25 bohr. The darkest regions corresponds to the bond axis while the lightest is 0.75 bohr from the bond axis.

Table 2. Stationary Points (bohr) for the Core Region of the Total Radial Density along the Bond Axis^a

H–Li	1.080	H–Be	0.906	H–B	0.845	H–F	0.689
H–Mg	1.002	H–Cl	0.765	H–K	1.196	H–Ca	1.124
Li–H	0.365	Li–F	0.365				
	0.361		0.361				
Be–H	0.267	0.889	B–H	0.212	0.777		
	0.267	0.888		0.211	0.709		
C–O	0.175	0.571	O–C	0.131	0.406		
	0.176	0.530		0.131	0.397		
F–H	0.115	0.362	0.734	F–Li	0.116	0.357	0.745
	0.116	0.376	0.809		0.117	0.316	0.799
Mg–H	0.087	0.240	0.502	1.519			
	0.088	0.241	0.503	1.516			
Cl–H	0.062	0.152	0.316	0.921			
	0.063	0.154	0.317	0.876			
Cl–Cl	0.062	0.152	0.318	0.945			
	0.063	0.154	0.318	0.892			
K–H	0.057	0.132	0.273	0.721	1.121		
	0.056	0.132	0.273	0.724	1.107		
K–F	0.056	0.132	0.273	0.720	1.123		
	0.057	0.132	0.273	0.727	1.106		
Ca–H	0.053	0.123	0.255	0.661	1.012	2.143	
	0.054	0.124	0.256	0.662	1.013	2.118	

^a The first row is for the nonbonding region, and the second row is for the bonding region for atom A bonded to atom B.

assigned relative weights for each atom's contribution to the molecular density at a given point. Spherical averaging of the weights for a specific atom at all points of radius r from the atomic nucleus defines the atomic contributions to the density at a given point in the next iteration. The cycle of defining new stockholder atoms followed by spherical averaging is repeated until the AIM densities converge. Stated benefits of this procedure include spherical atomic densities that add to exactly reproduce the molecular density, no promolecule generation requirement, no noted dependence on the choice of arbitrary initial weights used, no regions of negative density, and a simplicity of implementation relative to the Hirshfeld-I method of Bultinck, though Bultinck¹⁹ disagrees on this point in terms of comparison of the scaling of computational cost to implement the ISA method for larger molecules.

Furthermore, Bultinck¹⁹ found in a comparison of the Hirshfeld-I and ISA²⁰ approaches that atomic charges found via the

Table 3. Bond Lengths, Bond Critical Points (BCP), and Bond Maxima (B_{\max}) (bohr)

bond	R_{AB}	from atom	BCP	B_{\max}
H–Li	3.015	H	1.366	0.915
		Li	1.660	2.100
H–Be	2.521	H	1.437	0.826
		Be	1.084	1.695
H–B	2.246	H	1.271	0.778
		B	0.975	1.468
H–F	1.721	H	0.276	0.912
		F	1.445	0.809
H–Mg	2.245	H	1.581	1.742
		Mg	1.665	0.503
H–Cl	2.393	H	0.696	0.915
		Cl	1.697	1.478
H–K	4.389	H	1.865	1.269
		K	2.519	3.120
H–Ca	3.942	H	1.652	2.929
		Ca	2.290	1.013
C–O	2.105	C	0.694	1.198
		O	1.411	0.907
Li–F	2.938	Li	1.134	2.139
		F	1.804	0.799
F–K	4.130	F	1.991	1.106
		K	2.139	3.024
Cl–Cl	3.760	Cl	1.880	1.880

two methods are quite similar. Bultinck was also able to provide mathematical proofs that both the Hirshfeld-I and ISA approaches will yield unique AIM densities regardless of the initial promolecule choice (Hirshfeld-I) or initial stockholder weights (ISA) used.

While spherical AIMs are appealing due to their ability to be compared directly to spherical free atoms, there are legitimate concerns in their potential uses. For example, while a spherical AIM partitioning such as the ISA approach can reproduce the molecular density from which the AIM were generated, it can be argued that the spherical averaging of the technique smears out differences in electron density from the bonding and nonbonding regions of a molecule at a given radial distance from an atom in such a way that would reduce the transferability of AIM to build larger molecules, where these bonding

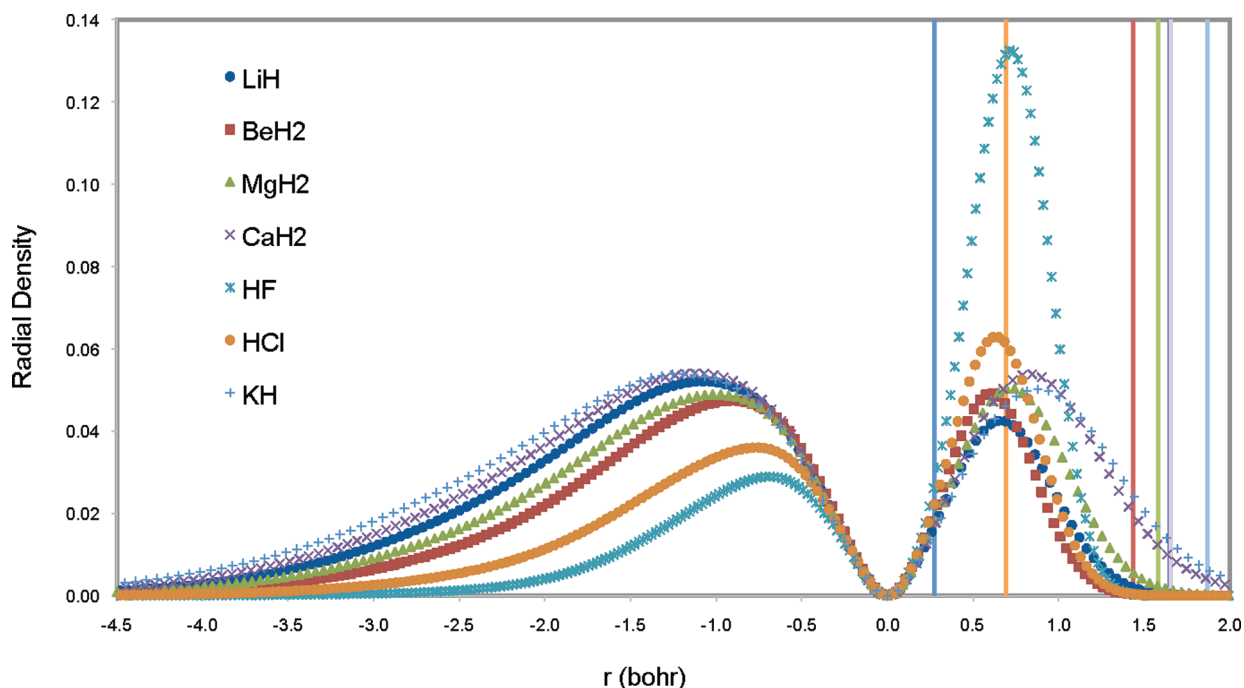


Figure 4. Radial densities for H (0.0) along the H–X bonds. The vertical lines correspond to the bond critical points.

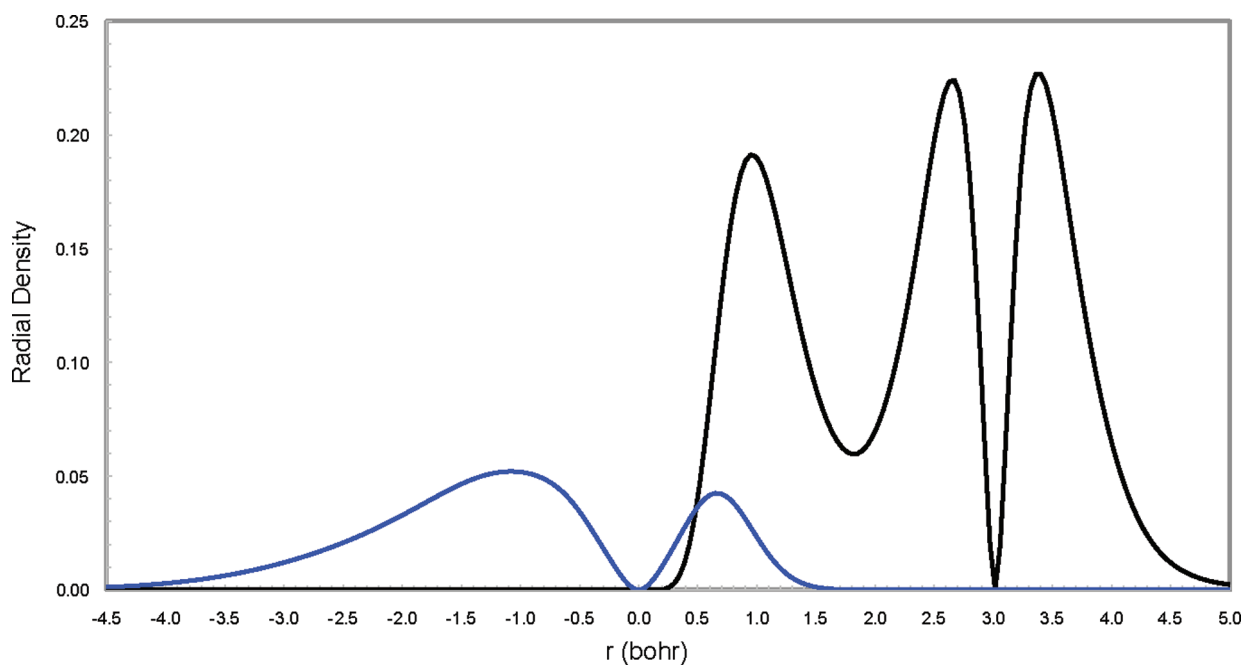


Figure 5. Radial densities for H (0.0) and Li (3.015) along the H–Li bond in LiH.

and nonbonding regions are localized differently in perhaps subtle, but meaningful ways. Parr describes this as a “Pauling-like way to envision AIM”, where an atom in a molecule is not a spherically symmetric ground-state atom, but rather an atom that undergoes changes in shape due to hybridization, promotion and charge transfer.²¹ As examples, it has been shown that direct addition of free atomic densities to create a larger molecule (equivalent to the Hirshfeld promolecule) generally results in a model that shows significant lack of similarity to a directly calculated electron density representation of the

molecule²² and Mayer⁵ counters with a nonspherical AIM concept that evaluates not only the net atomic populations of AIM but also the overlap populations of the interacting fuzzy AIM, which then gives information about bond orders and atomic valences.

One of the first properties that AIM are used to describe are atomic charges, usually in relation to describing molecular dipole moments. Bader²³ has outlined the criticisms of QTAIM atomic charges and molecular dipoles, while countering with his assessment of atomic charges arrived at using fuzzy AIM approaches⁴

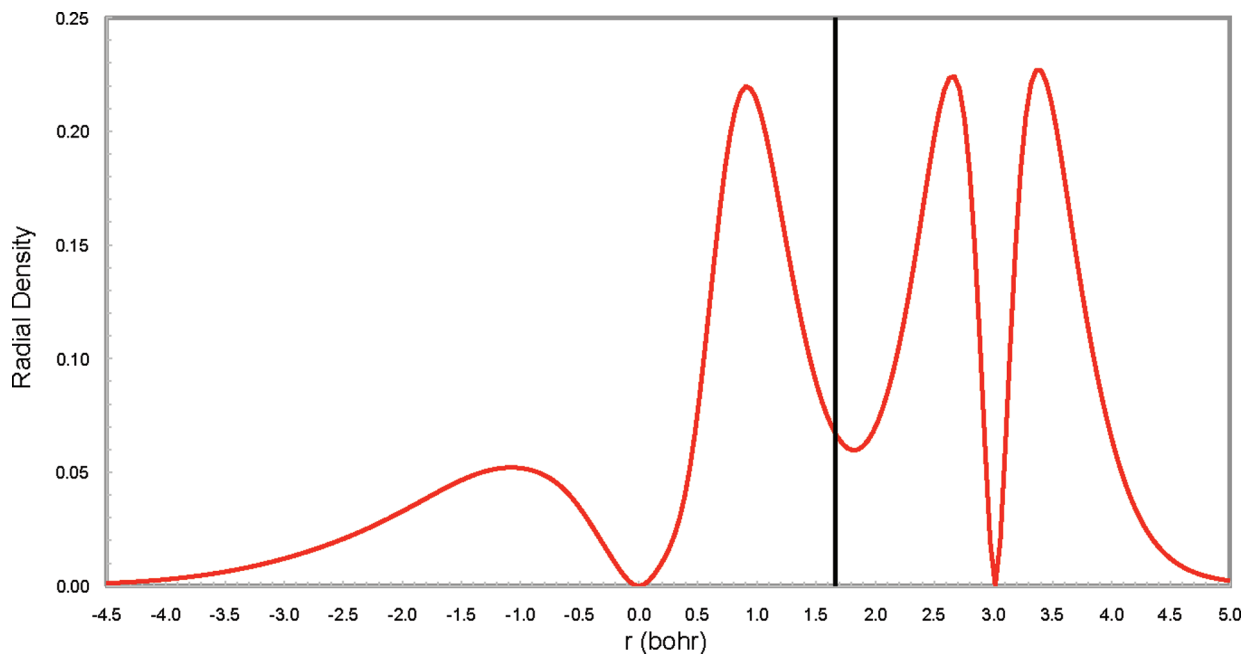


Figure 6. Total radial density along the H–Li bond in LiH. The solid line corresponds to the bond critical point.

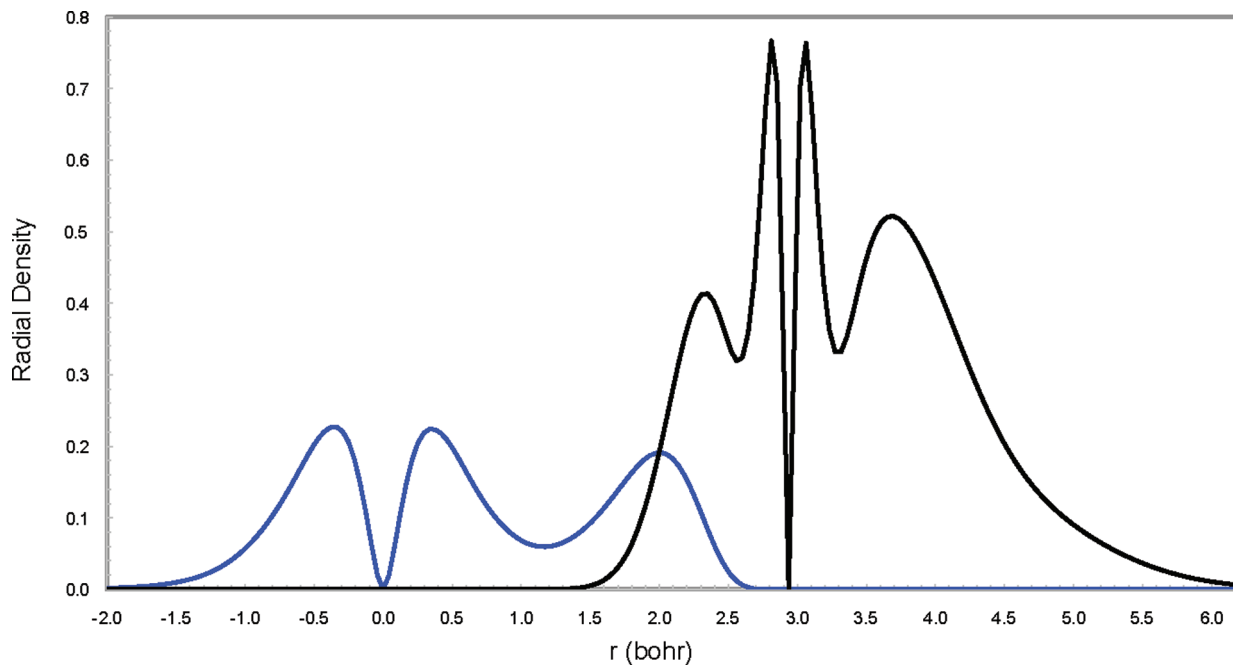


Figure 7. Radial densities for Li (0.0) and F (2.938) along the Li–F bond in LiF.

and Mulliken population analysis.¹⁰ He argues that overlapping AIM are unable to replicate the charges of atoms in ionic compounds due to the sharing of electron density that results for fuzzy AIM partitioning.

However, the main criticism of QTAIM atomic charges are that they are “too large” within the atomic basin (the volume of space within the zero-flux surface that encloses the nucleus) and result in calculated molecular dipole moments that are correspondingly too large. For example, carbon monoxide, calculated at the B3LYP/6-311G(3d,3p)//B3LYP/6-311G(3d,3p) level of

theory, has an oxygen charge (-1.13 e compared to a free oxygen atom) that results in a dipole moment which is too large and has the wrong sign (-6.08 D) compared to the experimentally measured dipole (0.11 D).²⁴ Furthermore, QTAIM charges calculated at the same level of theory²⁴ for the heavy atoms in HF (-0.713 e) and HCl (-0.233 e) give dipole moments (-3.15 and -1.43 D) that differ from the experimental magnitudes of 1.83 and 1.11 D , respectively.

To counter the discrepancies in dipole moments from the large atomic basin charges, Bader^{2,23,25} proposed that the calculated

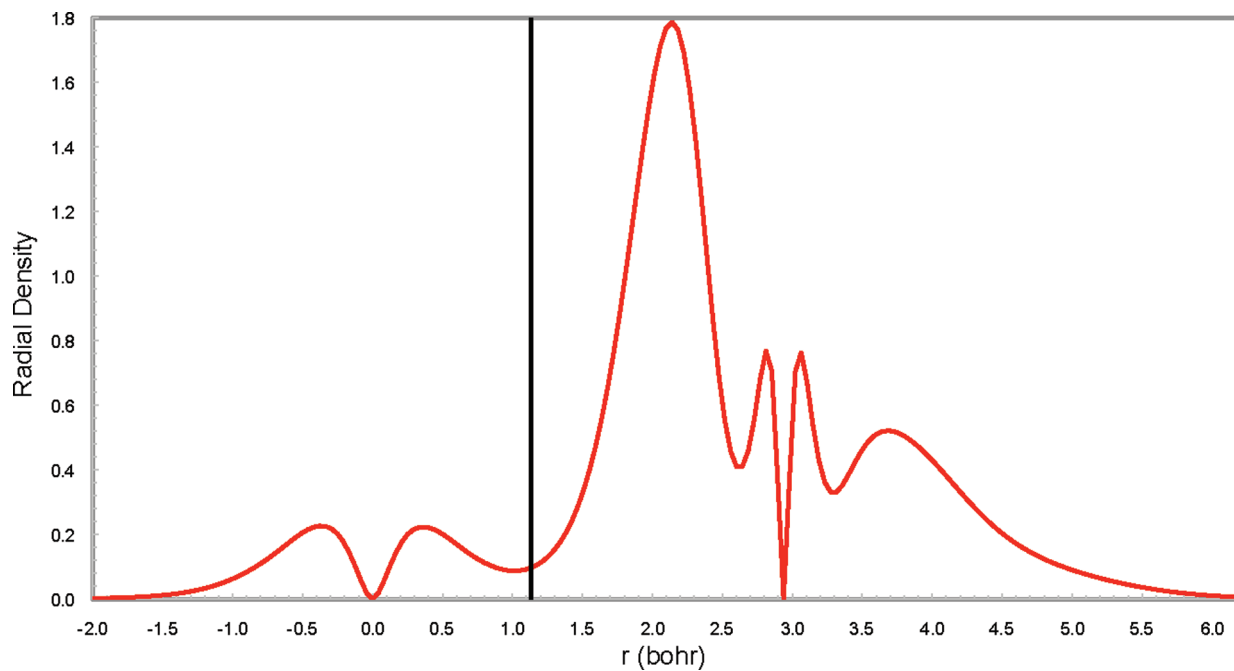


Figure 8. Total radial density along the Li–F bond in LiF. The solid line corresponds to the bond critical point.

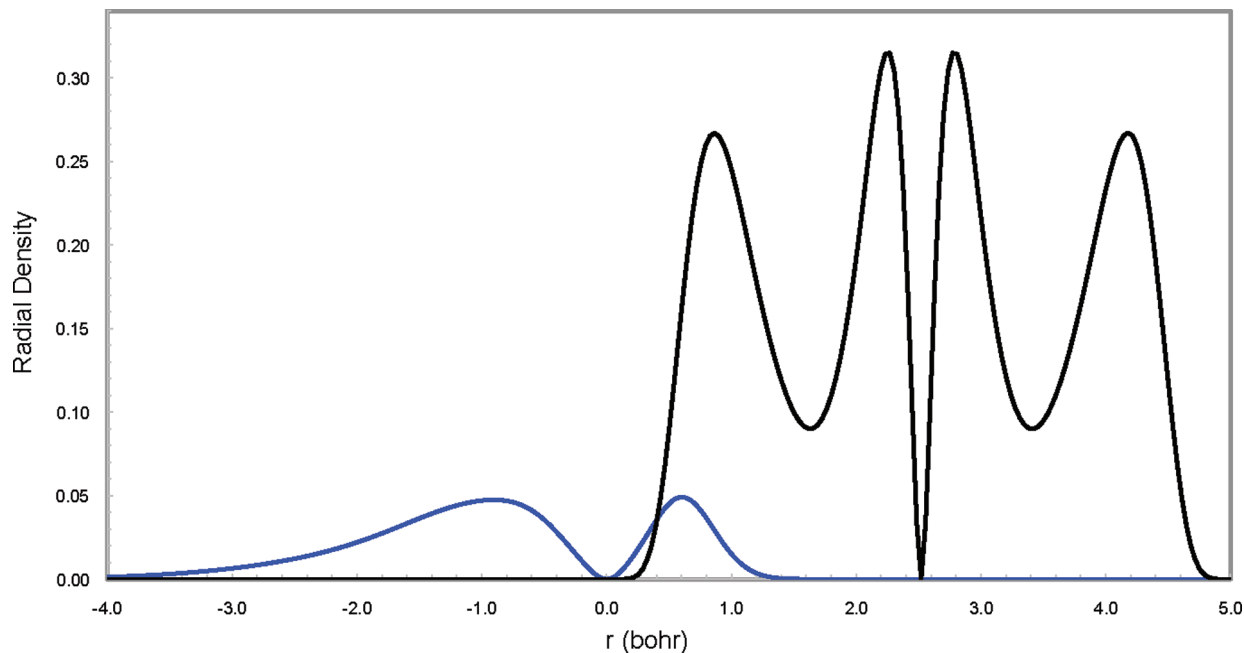


Figure 9. Radial densities for H (0.0) and Be (2.521) along the H–Be bond in BeH₂.

dipole moment cannot be evaluated by considering the atomic basin charges alone. While the atomic basin charges reflect the charge transfer that occurs between the zero-flux surfaces of the atoms in the molecule, condensing the total charge (nuclear and electronic) within the atomic basin to a point located at the nucleus is not sufficient to describe the contributions to the dipole moment by QTAIM. Instead, Bader suggests that the charge transfer through the zero-flux surface between the atoms will be accompanied by a counterpolarization of the QTAIM atomic densities in a direction opposite to that of the charge transfer. Essentially, the QTAIM atoms have

their own individual dipole moments that should be accounted for in the molecular dipole calculation. For a molecule like carbon monoxide,²⁴ the 1.13 e charges on the C and O undergo counterpolarization that leads to atomic dipole contributions to the molecular dipole of 6.23 D in the direction opposite that of the point charge dipole, which would sum to a molecular dipole of 0.14 D. This result has the correct sign and relative magnitude to the experimental dipole moment for CO.

In this work we present a new approach to looking at AIM where the partitioning of atoms in molecules is accomplished in

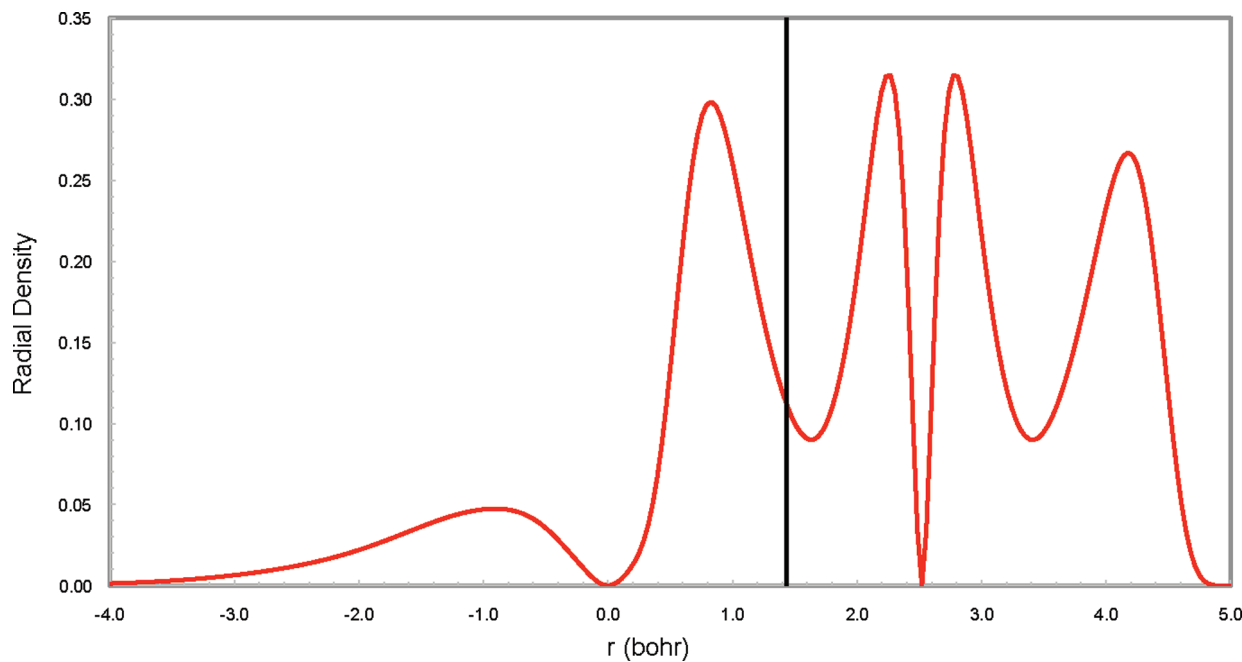


Figure 10. Total radial density along the H–Be bond in BeH_2 . The solid line corresponds to the bond critical point.

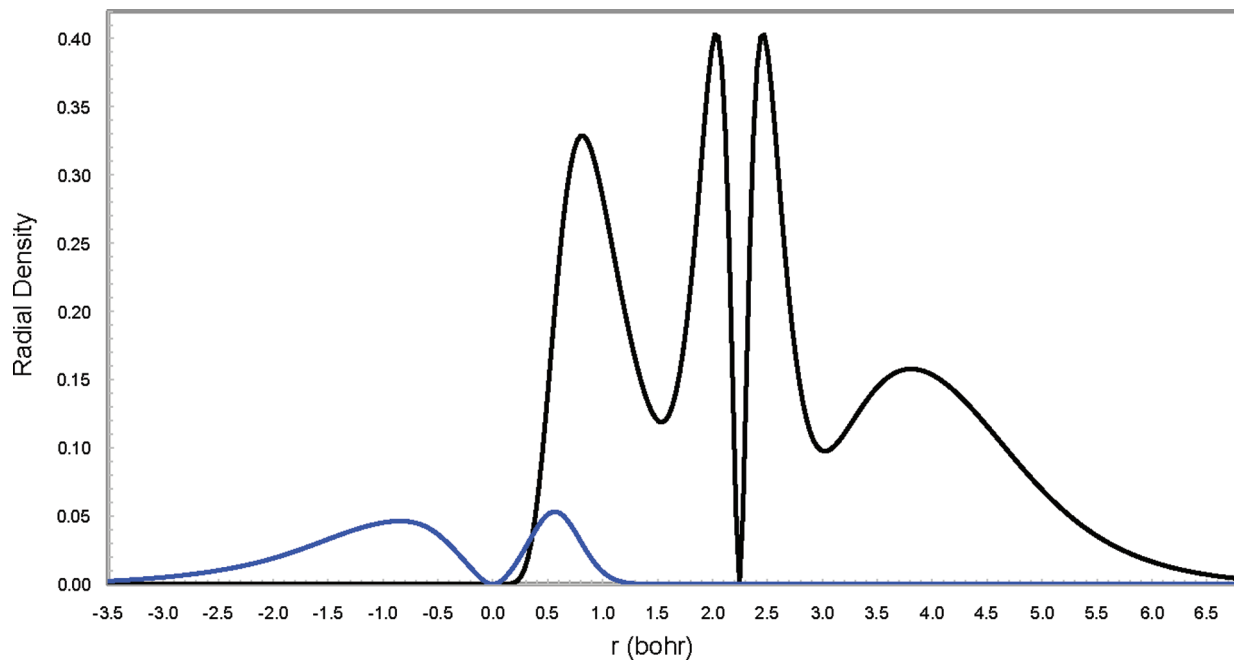


Figure 11. Radial densities for H (0.0) and B (2.246) along the H–B bond in BH_3 .

terms of atomic radial densities (AIMRD) and the total radial density (TRD). The results show that molecules can be partitioned into atomic regions and bonding regions. The atomic regions show radial densities that are very similar to those that would be encountered in isolated atoms.

■ COMPUTATIONAL METHOD

All the calculations were performed with program MUN-gauss.²⁶ The densities were calculated at the HF/6-31G(d)/HF/6-31G(d) level. For atoms it is generally more useful to

look at the radial density, $\rho(r)r^2$. For atoms in molecules we define the radial density of an atom A as $W_A \rho(r_A, \theta_A, \phi_A) r_A^2$, where W_A is the Becke weight²⁷ for atom A and r_A is the distance from atom A (for a fixed θ and ϕ). The Bragg–Slater radii used to determine the Becke weights are reported in Table 1. For this work, the radial densities are calculated along an axis defined by a given A–B bond (no angular dependence). This is illustrated in Figure 1 for CO. The total radial density along an axis defined by an A–B bond is given as $W_A \rho(r_A, \theta_A, \phi_A) r_A^2 + W_B \rho(r_B, \theta_B, \phi_B) r_B^2$. This is illustrated in Figure 2 for CO.

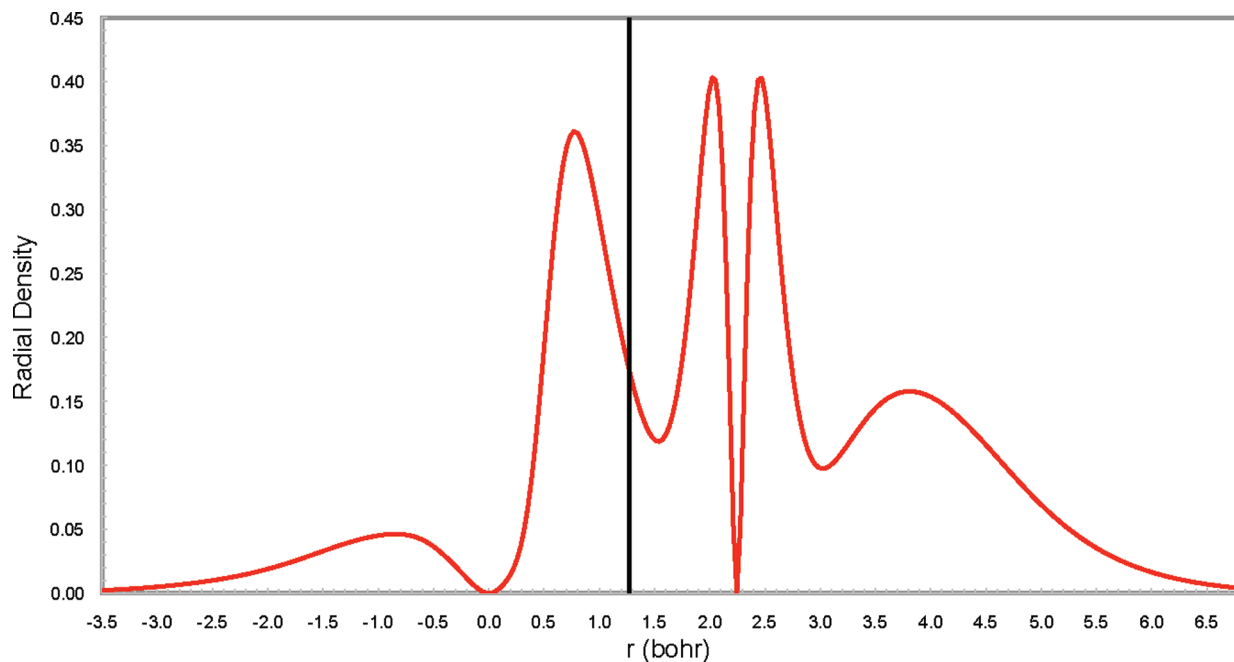


Figure 12. Total radial density along the H–B bond in BH_3 . The solid line corresponds to the bond critical point.

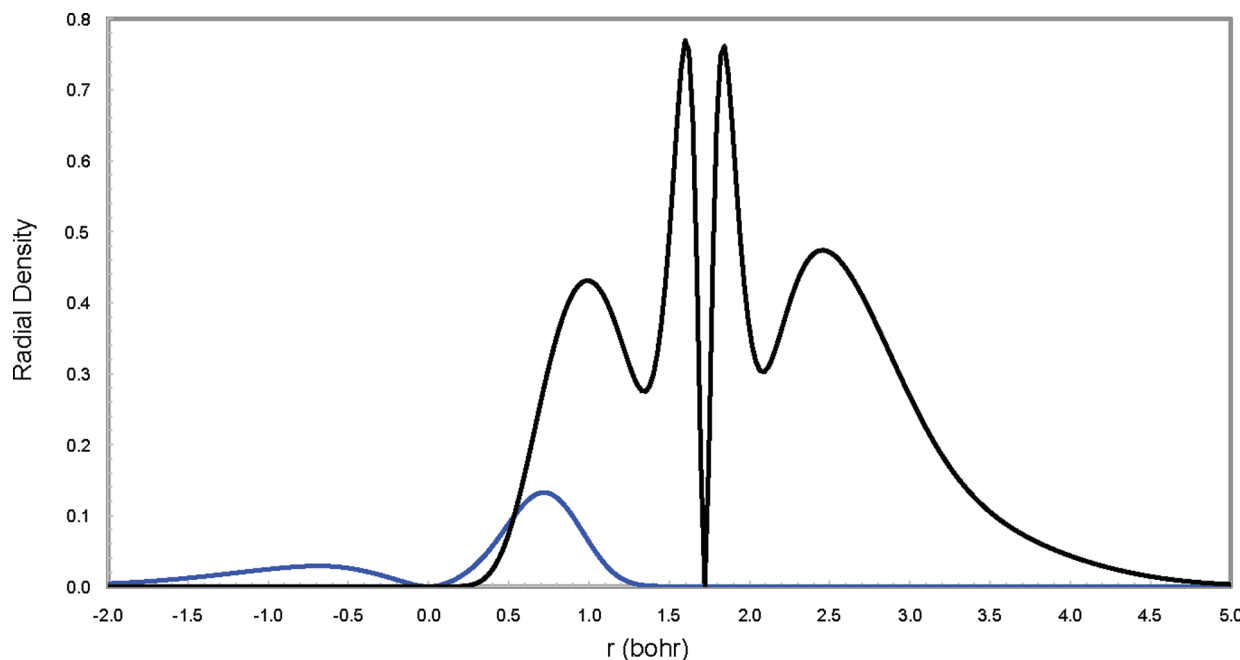


Figure 13. Radial densities for H (0.0) and F (1.721) along the H–F bond in HF.

■ RESULTS AND DISCUSSION

The AIM radial densities (AIMRD) and the total radial densities (TRD) for a number of bonds are given in Figures 2–26. The properties of the TRD are given in Tables 2 and 3.

AIM from Radial Densities. From the plots of the AIMRD it is interesting to note the atoms have shell structures and radial densities very similar to those found in individual atoms, with different number of maxima for first-, second- and third-row atoms. Table 2 lists the stationary points for the total radial

densities and Figure 4 compares the radial densities of the hydrogen atoms in different hydrides. The maximum radial densities in the nonbonding region (the points on the bond axis not in between the bonded nuclei) of the hydrogen atom correlate well with the amount of “hydride” character, where the radial density decreases in the order $\text{HK} > \text{HCa} > \text{HLi} > \text{HMg} > \text{HBe} > \text{HCl} > \text{HF}$, which is in order of increasing electronegativity of X. The maxima range from 0.689 bohr (HF) to 1.196 bohr (KH). The H atom in MgH_2 has a maximum at 1.002 bohr, which is very close to the 1s shell maximum of an individual

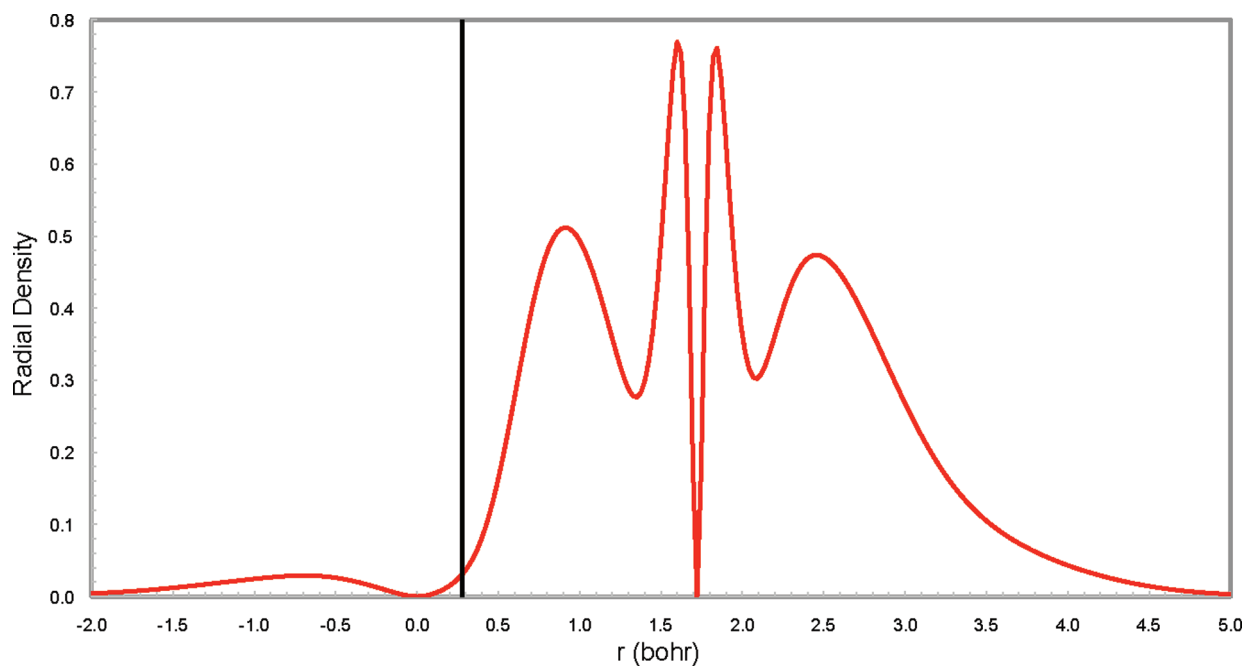


Figure 14. Total radial density along the H–F bond in HF. The solid line corresponds to the bond critical point.

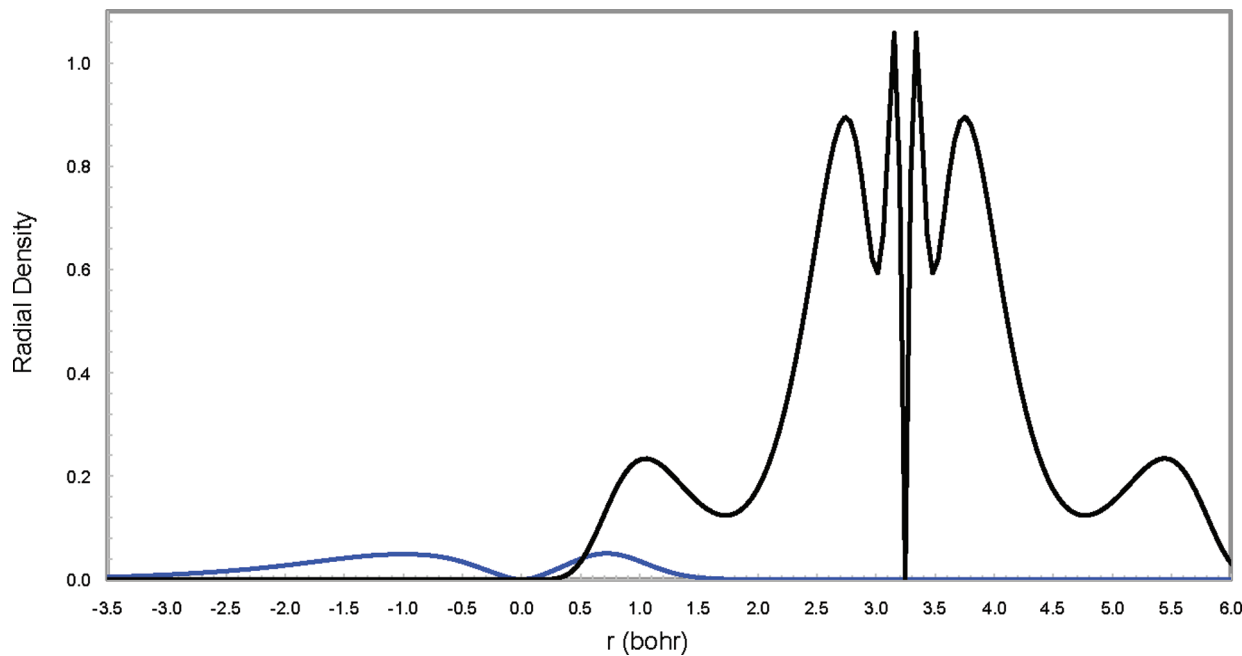


Figure 15. Radial densities for H (0.0) and Mg (2.245) along the H–Mg bond in MgH_2 .

hydrogen atom. For the bonding region between the two nuclei the maximum radial densities decrease in the order $\text{HF} \gg \text{HCl} > \text{HCa} \approx \text{HK} > \text{HMg} > \text{HBe} \approx \text{HLi}$.

For Li the maximum radial density in the nonbonding region is at 0.365 bohr for both LiH and LiF (Table 2, Figures 5 and 7). For Cl the stationary points in the nonbonding region are at 0.062, 0.152, 0.316, and 0.921 in HCl and at 0.062, 0.152, 0.318, and 0.945 in Cl_2 and (Table 2, Figures 17 and 19). The positions of the stationary points corresponding to core electrons in the bonding region are also fairly constant at 0.063, 0.154, 0.318, and 0.892 bohr in Cl_2 and 0.063, 0.154,

0.317, and 0.876 bohr in HCl. Similarly, for K in KH and KF (Table 2, Figures 21 and 23), the stationary points for the core electrons in both the bonding and nonbonding regions remain invariant at 0.056, 0.132, and 0.273. Only at larger radial distances from the K nucleus do slight variations in the position of the stationary points arise. In KH the nonbonding region sees these outer stationary points at 0.721 and 1.121, while in the bonding region these occur at 0.724 and 1.107. For KF these more distant stationary points are at 0.720 and 1.123 in the nonbonding region and 0.727 and 1.106 in the bonding region.

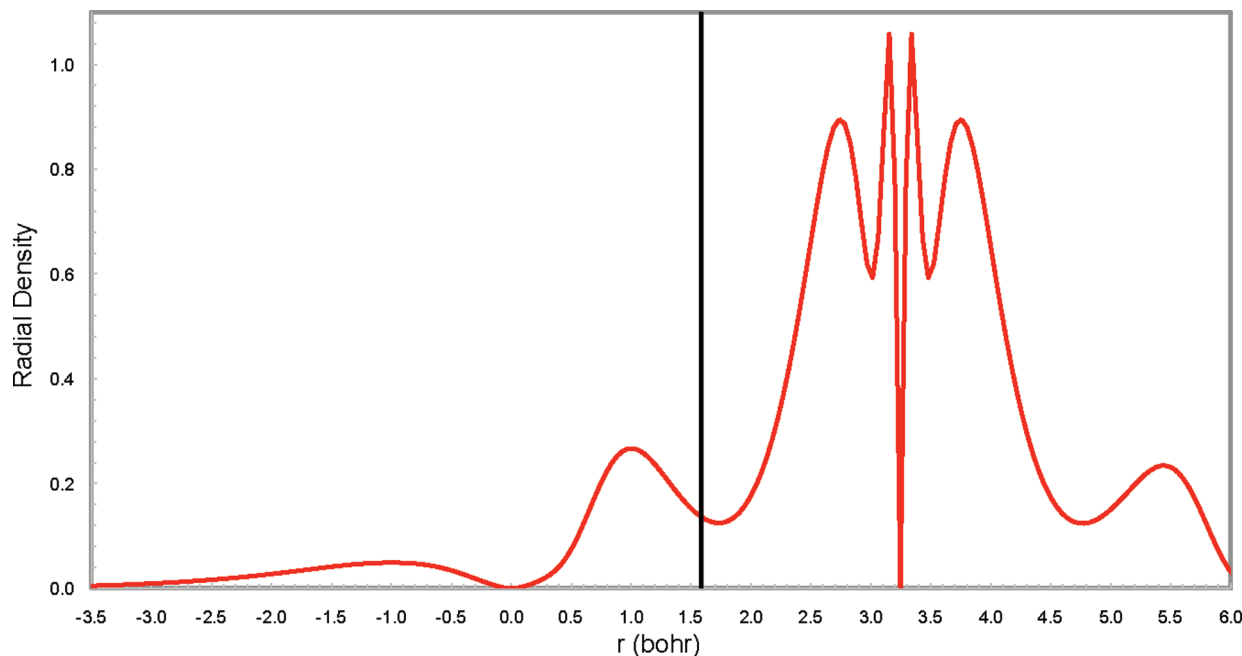


Figure 16. Total radial density along the H–Mg bond in MgH_2 . The solid line corresponds to the bond critical point.

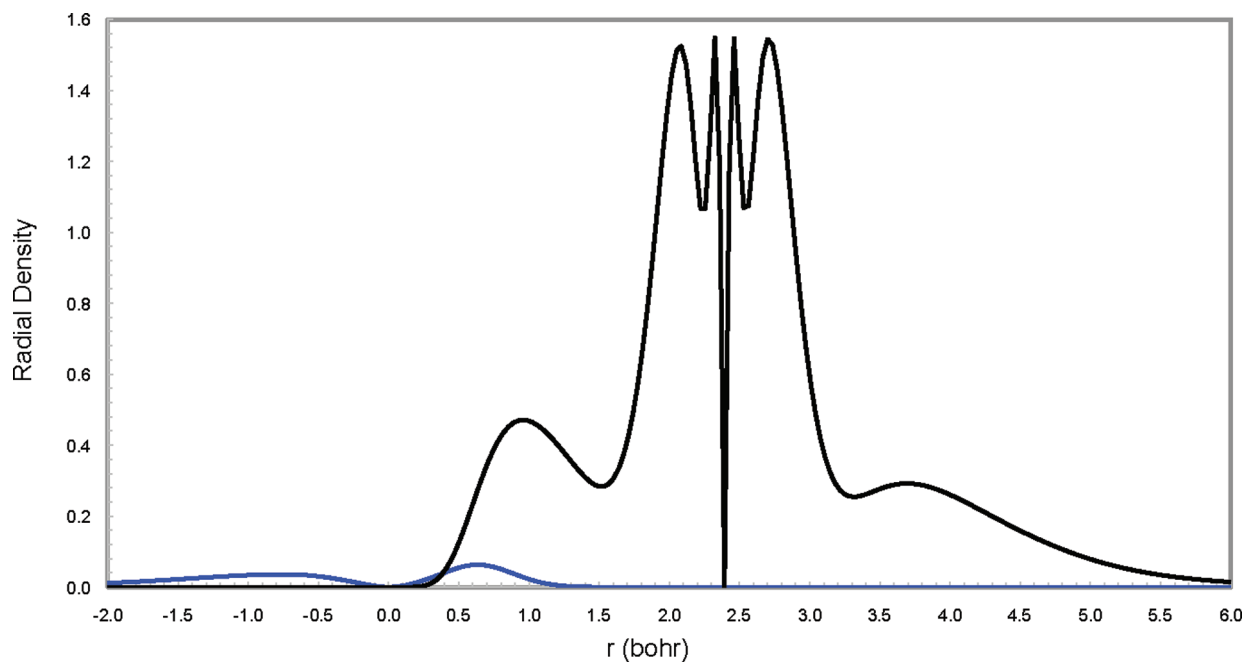


Figure 17. Radial densities for H (0.0) and Cl (2.393) along the H–Cl bond in HCl.

Bonds in Molecules from Radial Densities. The consistency of the positions of many of the stationary points for a given atom type in differing molecular environments in both the nonbonding and bonding regions allow for a new definition of AIM partitioning. We propose that unlike the QTAIM model, the AIMRD model will allow for partitioning of molecular density into effectively spherical core AIMs where the stationary points show no differences regardless of molecular environment, and a bonding region where two potentially nonspherical atomic valence shell regions overlap. Within this bonding region is found a maximum of total radial density, and as seen in Table 3, the

position of these maxima do not generally correspond with the bond critical point for most bonds, which is the boundary of the zero-flux region on the bond axis in the QTAIM method. The maxima of the TRD for the hydrides in the bonding region (Table 3) range from 0.778 bohr (H–B) to 1.269 bohr (H–K).

To visualize the TRD away from the CO bond axis, we plotted three axes parallel to the bond at incremental distances of 0.25 bohr (see Figure 3). The distances from a nucleus to the maxima in the TRD were calculated. For the carbon of CO, the distance to the maximum of the TRD in the bonding region occurs at 1.198 bohr on the internuclear axis (Table 3) but increases

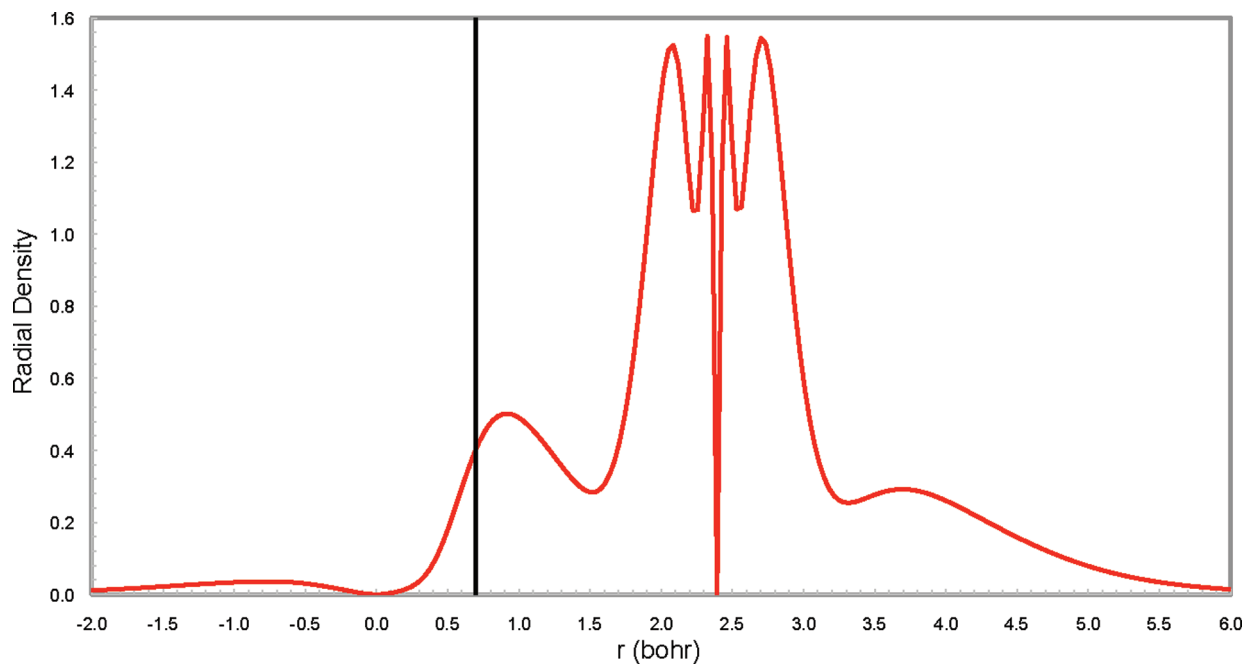


Figure 18. Total radial density along the H–Cl bond in HCl. The solid line corresponds to the bond critical point.

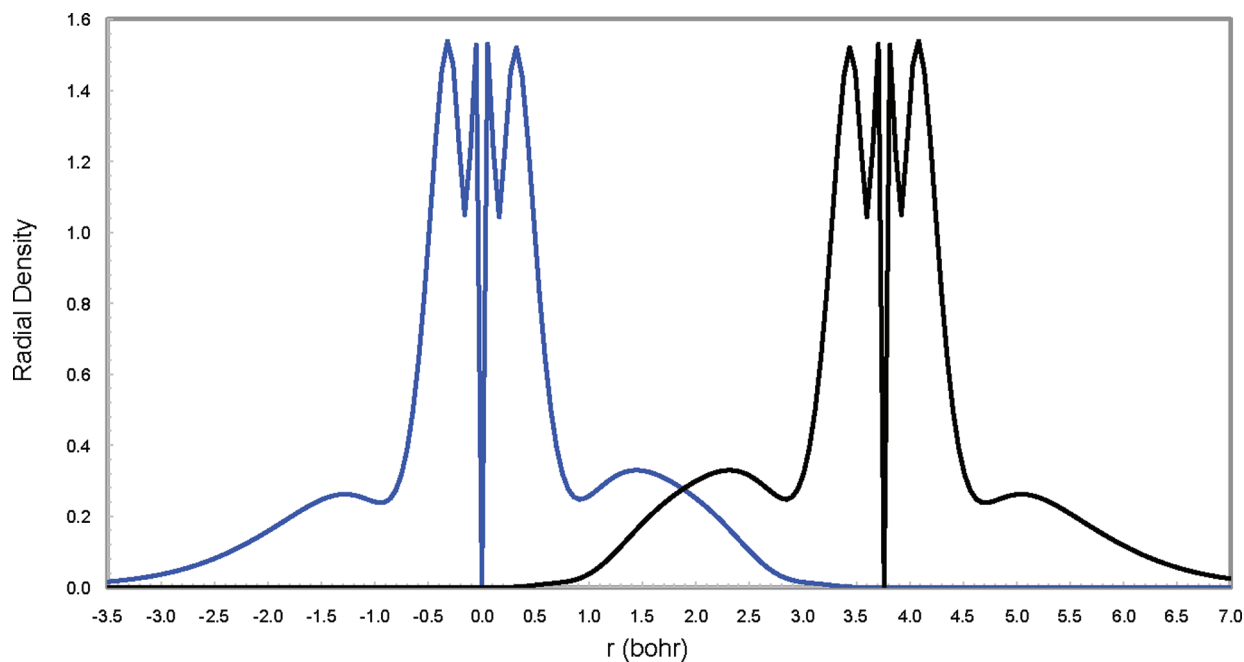


Figure 19. Radial densities for the Cl (0.0 and 3.760) atoms along the Cl–Cl bond in Cl₂.

steadily to 1.226, 1.304, and 1.424 bohr as we consider each shifted axis. The behavior of oxygen in the bonding region of CO mirrors this increase, with the distance to the TRD maxima increasing from 0.907 (Table 3) to 0.938, 1.030, and 1.207 bohr, respectively.

In the nonbonding region the carbon TRD maxima occur at distances of 1.187, 1.229, 1.345, and 1.512 bohr, respectively. When compared to the bonding region maxima for the same axes, it can be seen that the nonbonding maximum occurs at a shorter distance than the bonding region maximum along the bond, but as we shift away from the bond the nonbonding

maximum quickly occurs at a further distance from the nucleus than the bonding region maximum. This behavior indicates distortion of the carbon AIMRD from the spherical free carbon radial density due to the presence of the O. For oxygen, the TRD nonbonding maxima occur at 0.835, 0.883, 1.019, and 1.207 bohr, respectively. While the nonbonding region maximum once again occurs at a shorter distance from the nucleus compared to the bonding maximum along the bond axis, the nonbonding region maxima do not occur at further distances than the bonding region maxima. Rather, for the furthest axis considered from the bond, the distances from the oxygen nucleus are essentially equal

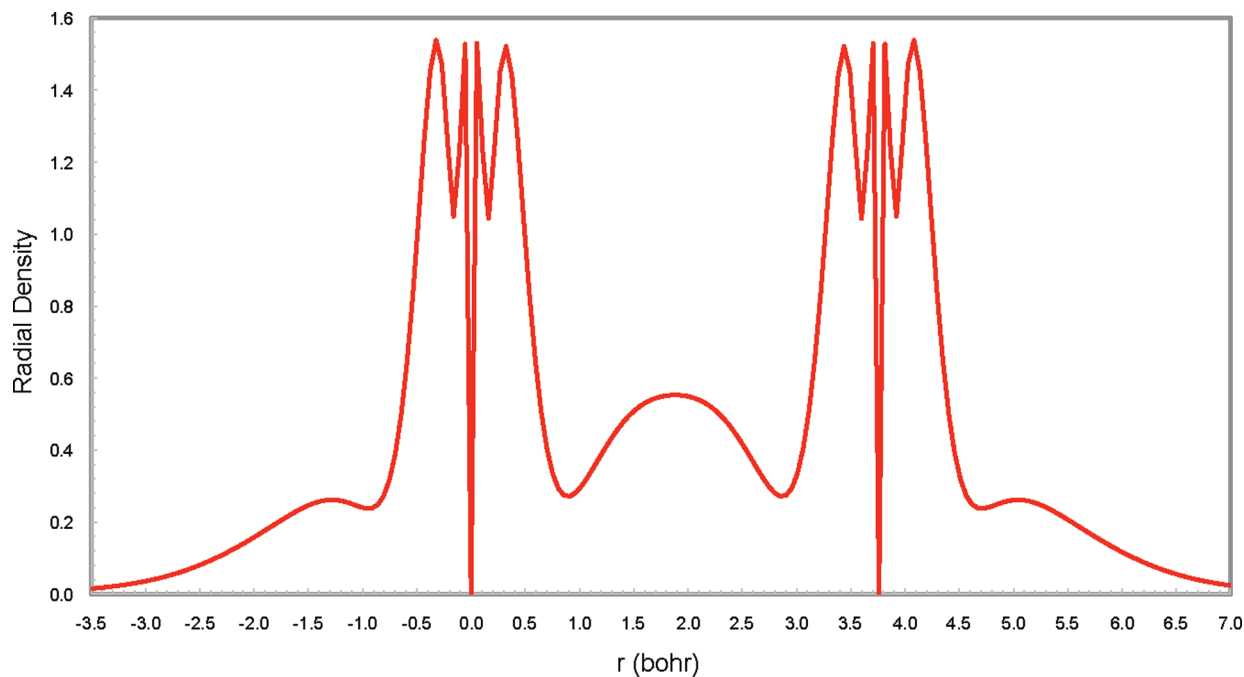


Figure 20. Total radial density along the Cl–Cl bond in Cl_2 .

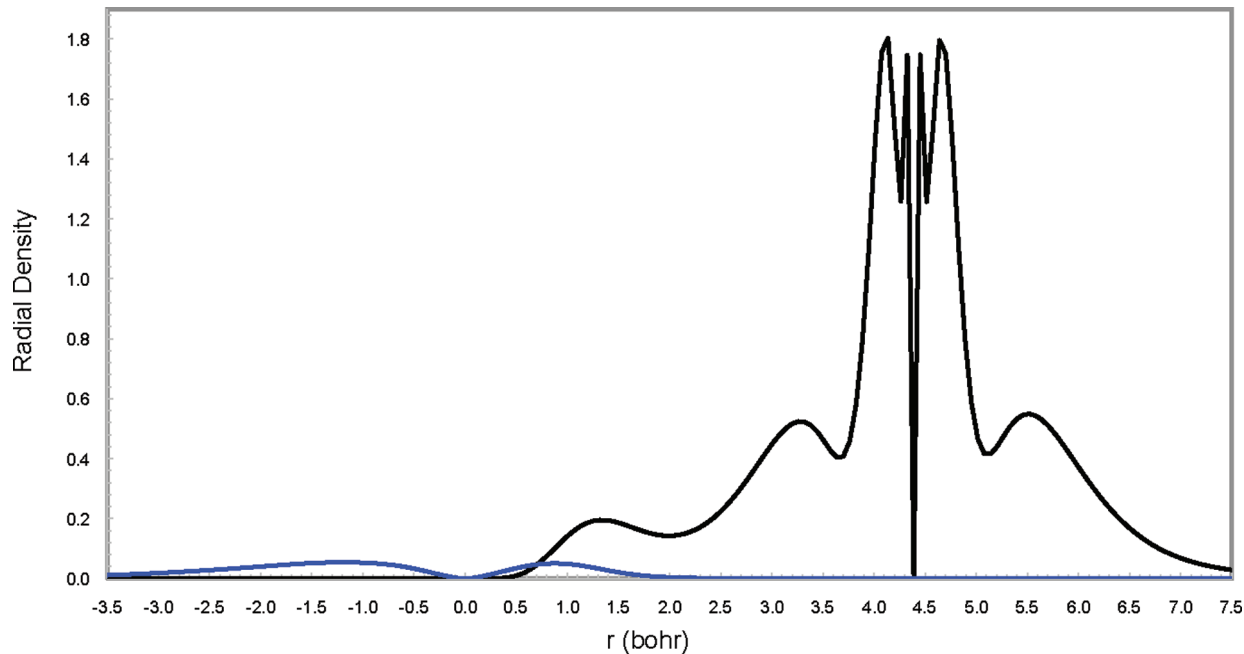


Figure 21. Radial densities for H (0.0) and K (4.389) along the H–K bond in KH.

for the bonding and nonbonding maxima. Therefore, the oxygen AIMRD is also distorted by the C atom. These observations are consistent with Parr's description of AIM undergoing change in shape relative to free atoms.²¹

The problem associated with the atomic charges obtained using QTAIM was noted in the Introduction. Carbon monoxide, for example, has an excess of electron density associated with the oxygen atom resulting in a dipole moment that is too large and that has the wrong sign. This is evident from Figure 2 where the BCP is close to carbon, implying that most of the molecular electron density is being assigned to the oxygen atomic basin.

Based on the AIMRD and TRD, it would seem more reasonable to shift the boundary to the maximum radial density in the bonding region, which is closer to the oxygen atom (at ~ 1.20 bohr, Figure 2). This would give more of the molecular density to the carbon atom, and should lead to a significant reduction of the magnitude of the charges associated with each atom.

To test the validity of using the Becke weight in calculating AIM properties, we calculate the net atomic charges by integrating the HF/6-31G(d) density numerically and calculate the dipole moment using the resulting net atomic charges. Using the standard Bragg–Slater radii ratio, the net atomic charge for

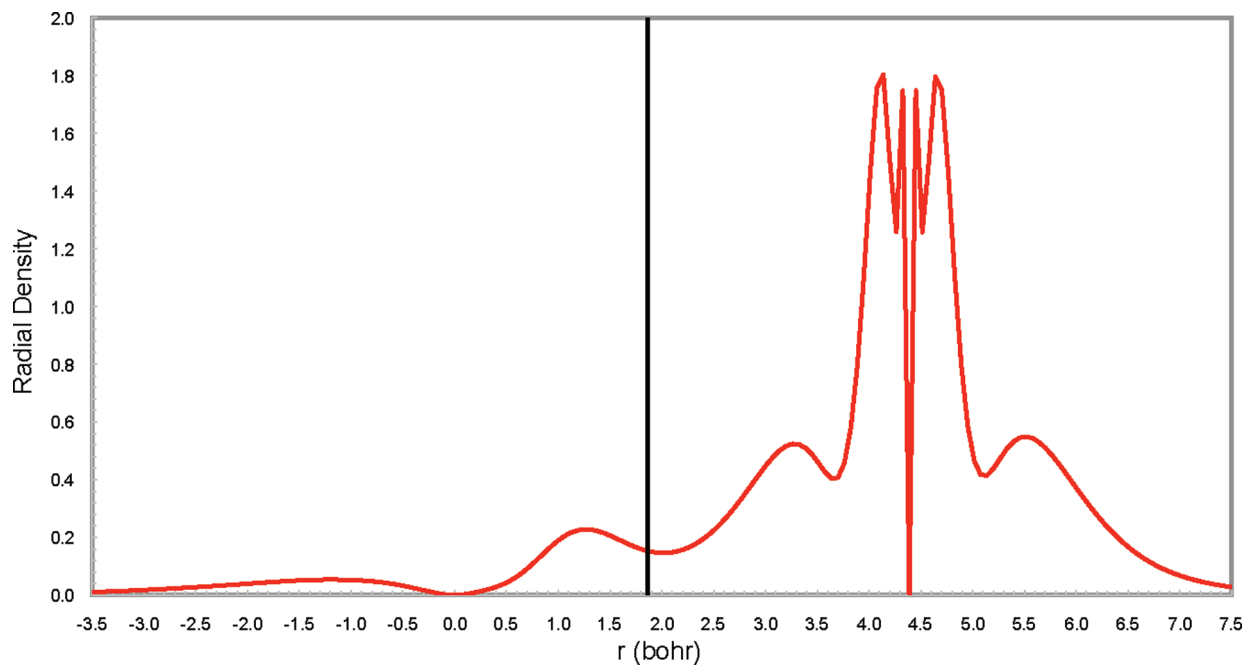


Figure 22. Total radial density along the H–K bond in KH. The solid line corresponds to the bond critical point.

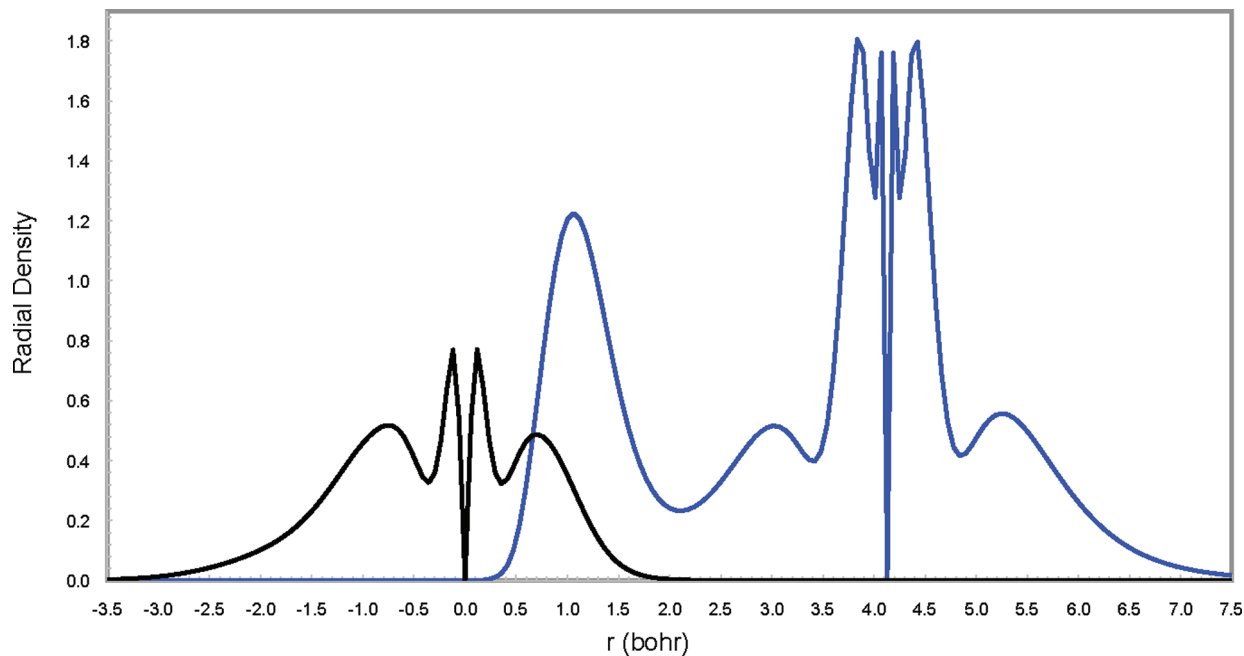


Figure 23. Radial densities for F (0.0) and K (4.130) along the F–K bond in KF.

carbon in CO is -0.070 e with a resulting dipole moment of 0.372 D with the correct sign. Whereas, when the Bragg–Slater radii ratio is set to 1, the net atomic charge on carbon is $+0.190\text{ e}$ with a dipole of 1.017 D in the opposite direction. This suggests that with the proper Bragg–Slater ratio the Becke weight can be a reliable way of partitioning the density into AIM.

If we continue taking the maximum where the two AIMRD overlap as the dividing boundary between two atoms, the boundary would be shifted closer to the hydrogen atom for LiH (Figures 5 and 6), BeH (Figures 9 and 10), BH (Figures 11 and 12), MgH (Figures 15 and 16), KH (Figures 21 and 22), and

CaH (Figures 25 and 26). For LiF (Figures 7 and 8), HF (Figures 13 and 14), HCl (Figures 17 and 18), and KF (Figures 23 and 24), the boundary would be shifted closer to the halogen atom in all cases, in comparison to the QTAIM bond critical point. This shift would result in more of the molecular density being assigned to the hydrogen atoms of HCl and HF, for example, which would result in lower charge and dipole magnitudes in comparison to the QTAIM method.

Additionally, the AIMRD show a distinct trend that follows the combined trends of the transition from ionic bonding to covalent bonding in the hydrides, and the relative electronegativity

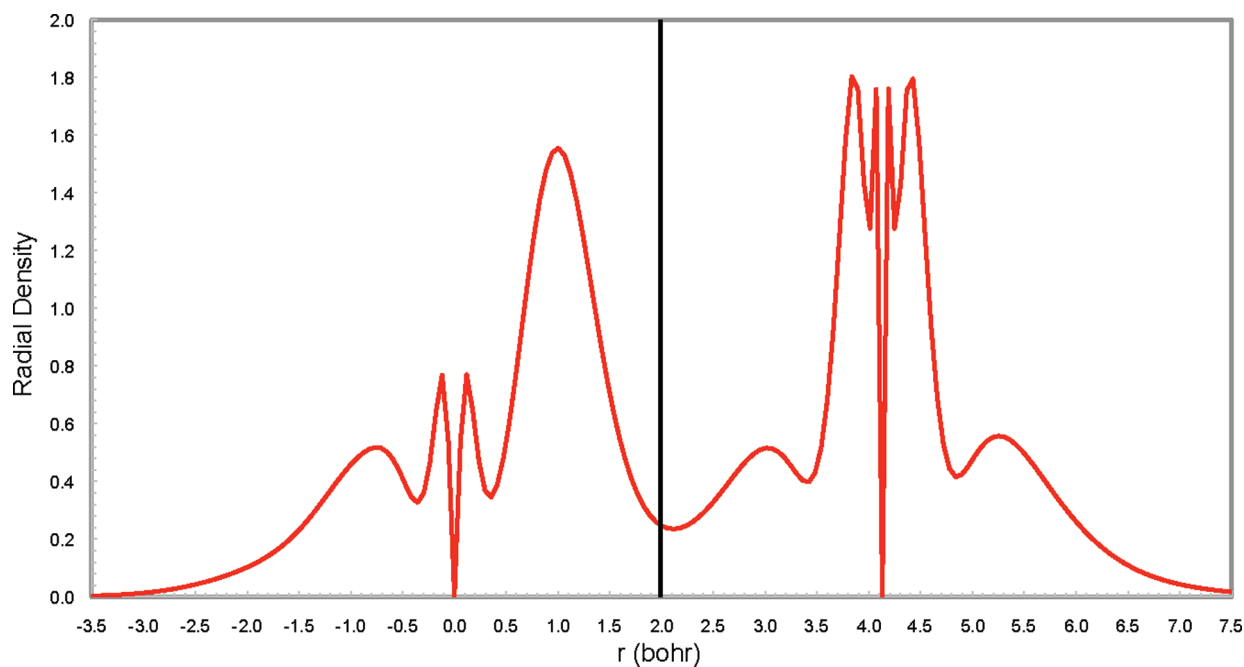


Figure 24. Total radial density along the F–K bond in KF. The solid line corresponds to the bond critical point.

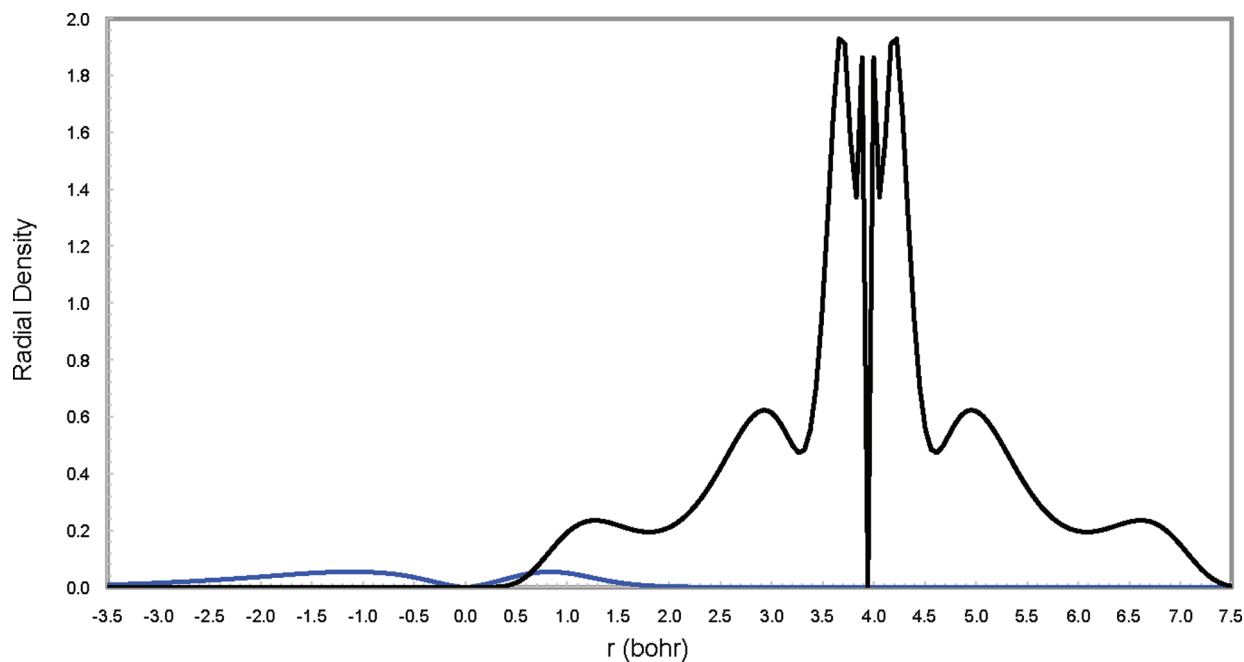


Figure 25. Radial densities for H (0.0) and Ca (3.942) along the H–Ca bond in CaH_2 .

of the atom bonded to hydrogen. If the AIMRD of LiH (Figure 5), LiF (Figure 7), and HF (Figure 13) are considered, we see that a Li atom in both LiH and LiF does not show a second shell in the nonbonding region, but does in the bonding region, while the fluorine atom in HF and LiF shows a second shell in both regions and the atomic maximum radial density of this second shell is larger in the nonbonding region as compared to in the bonding region. These observations indicate that the LiH and LiF bonds are more ionic in character than the HF bond, since an electron is essentially not found in the lithium 2s shell except where the 2s overlaps with the

outer shell of the other atom. In HF there is an indication of sharing of electrons from both atoms outer shells, but the electronegative fluorine pulls some of this shared density toward itself. Similar behavior can be noted again in the potassium atoms of KH (Figure 21) and KF (Figure 23): only three shells are seen in the nonbonding region, while four are seen in the bonding region. This gives an indication of the ionic character of potassium in these molecules.

Dependence of AIM Radial Densities on Becke Weights. For AIMRD, like any other definition of AIM, the partitioning of the total electron density into atomic contributions is arbitrary.

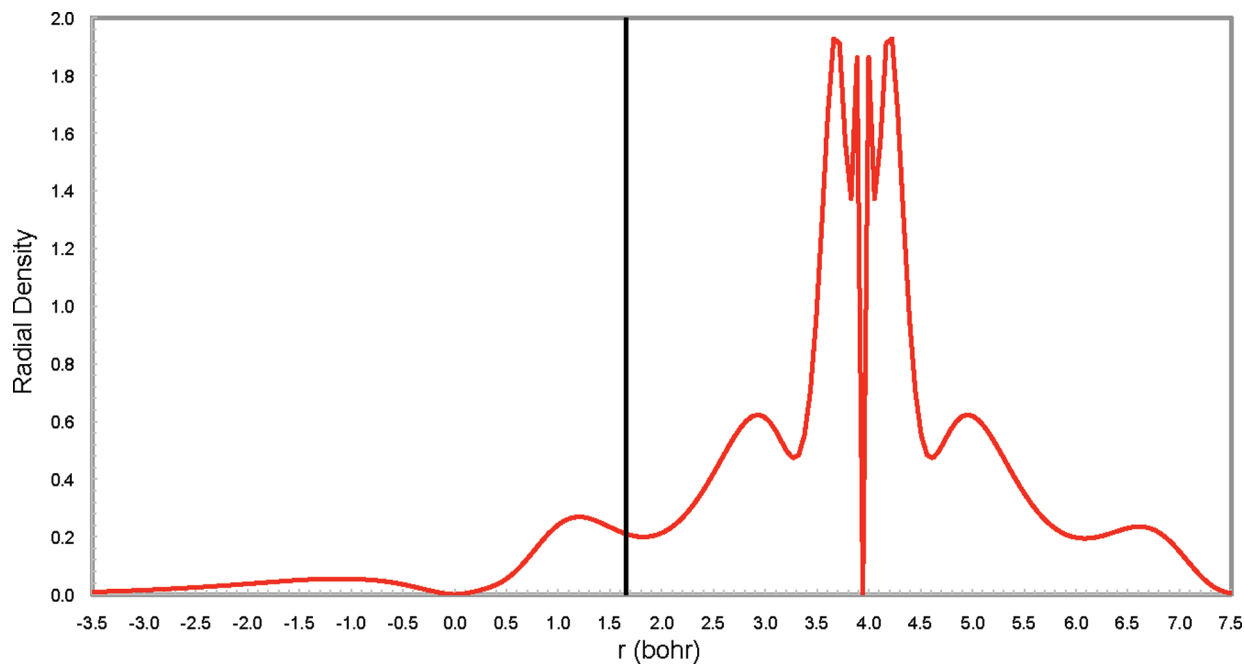


Figure 26. Total radial density along the H–Ca bond in CaH_2 . The solid line corresponds to the bond critical point.

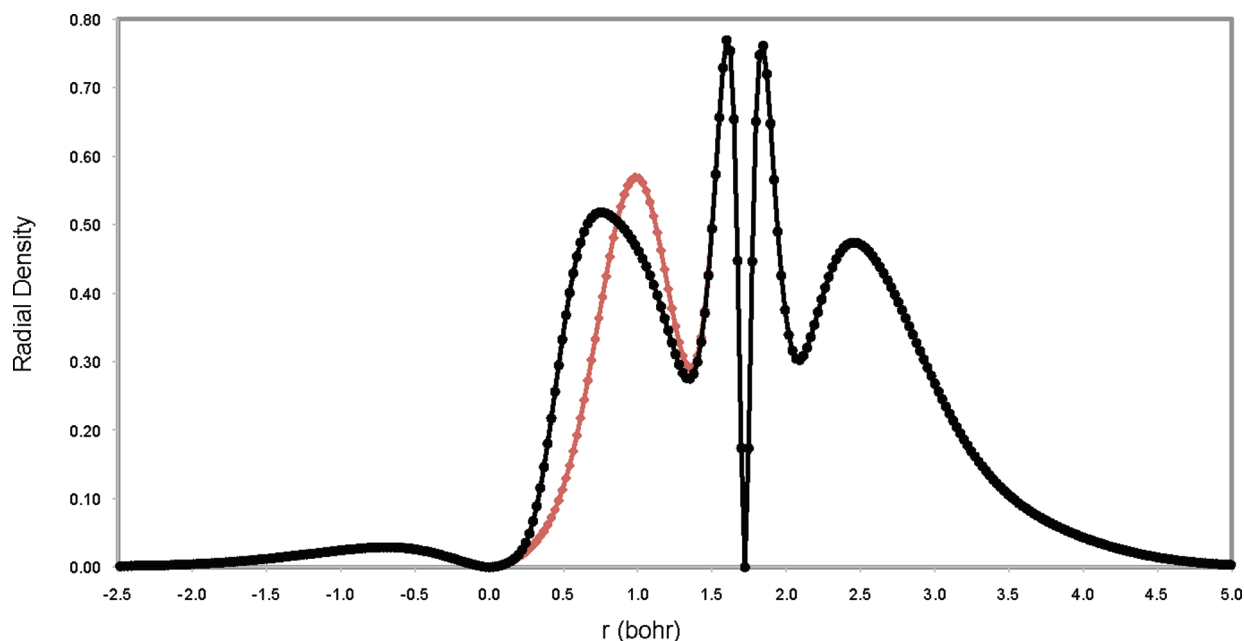


Figure 27. Total radial density along the H–F bond in HF for two different ratios of the Bragg–Slater radii, $R_{\text{F}}/R_{\text{H}} = 1.0$ (red) and $R_{\text{F}}/R_{\text{H}} = 2.4$ (black).

In this case the partitioning will depend on the ratio of the Bragg–Slater radii ($\chi_{ij} = R_i/R_j$) used to define the Becke weight. The total TRD for HF (Figure 27) and LiH (Figure 28) are plotted for two different values of χ_{ij} , $R_X/R_{\text{H}} = 1.0$ and $R_X/R_{\text{H}} = 2.4$. Although the total electron density is invariant, the radial density shifts from H to F in HF and from H to Li in LiH as the ratio increases. The position of the TRD maximum also changes. Note that only the overlap region is affected by χ_{ij} . The AIM and bonds in molecules (BIM) regions appear to be unaffected by the ratio. As such, if the core stationary points of the radial density remain invariant regardless of the molecular environment, the

ratio used to define the Becke weight can be set as the ratio of the radii of the furthest core shells of the atoms. This would remove the dependence of defining the Becke weight on a fixed table of atomic radii.

An alternative approach also being explored is one where the ratio of radii is arbitrarily set to an initial value and ratio of the distances from the bonded nuclei to the TRD maximum is used to revise the radii ratio. The process can then be iterated until the position of the TRD maximum and the ratio become invariant. Such a process would be consistent with Slater's notion²⁸ that an atomic radius can be set to the radial distance of the outermost

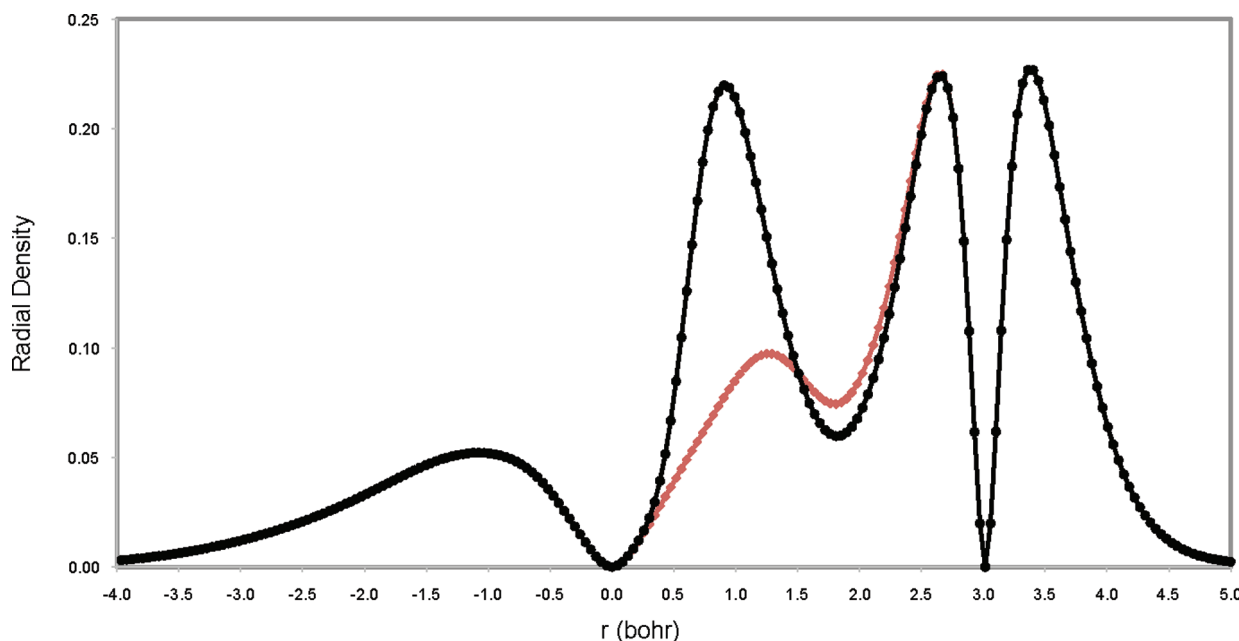


Figure 28. Total radial density along the H–Li bond in LiH for two different ratios of the Bragg–Slater radii, $R_{\text{Li}}/R_{\text{H}} = 1.0$ (red) and $R_{\text{Li}}/R_{\text{H}} = 2.4$ (black).

shell of the atom, and bonding occurs where there is a maximal overlap of these outermost shells.

CONCLUSIONS

These preliminary findings suggest that AIM radial densities and total radial densities may provide more detail and more intuitively help partition the density to not only define atoms in molecules (AIM) but also to define BIM. Radial densities for atoms in molecules are quite similar to those in individual atoms. It may thus be possible to more easily fit radial densities of AIM to generate total molecular densities. Although dependent on the Becke weight, the maximum in radial density in the bond region may provide a better partitioning of the molecular density into atomic contributions.

AUTHOR INFORMATION

Corresponding Author

*E-mail: P.L.W., peterw@mun.ca; R.A.P., rpoirier@mun.ca

ACKNOWLEDGMENT

We gratefully acknowledge the support of the Natural Sciences and Engineering Council of Canada and the Atlantic Excellence Network (ACEnet) for the computer time.

REFERENCES

- (1) Moffitt, W. *Proc. R. Soc. London, Ser. A* **1951**, *210*, 245–268.
- (2) Bader, R. F. W. *Atoms in Molecules: A Quantum Theory*; Clarendon: Oxford, U.K., 1990.
- (3) Stewart, R. F. *J. Chem. Phys.* **1970**, *53*, 205–213.
- (4) Hirshfeld, F. L. *Theor. Chim. Acta* **1977**, *44*, 129–138.
- (5) Mayer, I.; Salvador, P. *Chem. Phys. Lett.* **2004**, *383*, 368–375.
- (6) Bultinck, P.; Alsenoy, C. V.; Ayers, P. W.; Carbó-Dorca, R. J. *Chem. Phys.* **2007**, *126*, 144111.
- (7) Lillestolen, T. C.; Wheatley, R. J. *Chem. Commun.* **2008**, 5909–5911.
- (8) Matta, C. F.; Bader, R. F. W. *J. Phys. Chem. A* **2006**, *110*, 6365–6371.
- (9) Bader, R. F. W. *J. Phys. Chem. A* **2010**, *114*, 7431–7444.
- (10) Mulliken, R. S. *J. Chem. Phys.* **1955**, *23*, 1833–1840.
- (11) Gill, P. M. W. *J. Phys. Chem.* **1996**, *100*, 15421–15427.
- (12) Yáñez, M.; Stewart, R. F.; Pople, J. A. *Acta Crystallogr.* **1978**, *A34*, 641–648.
- (13) Lee, A. M.; Gill, P. M. W. *Chem. Phys. Lett.* **1998**, *286*, 226–232.
- (14) Gilbert, A. T. B.; Lee, A. M.; Gill, P. M. W. *J. Mol. Struct.: THEOCHEM* **2000**, *500*, 363–374.
- (15) Gilbert, A. T. B.; Gill, P. M. W.; Taylor, S. W. *J. Chem. Phys.* **2004**, *120*, 7887–7893.
- (16) Davidson, E. R.; Chakravorty, S. *Theor. Chim. Acta* **1992**, *83*, 319–330.
- (17) Bultinck, P.; Ayers, P. W.; Fias, S.; Tiels, K.; Alsenoy, C. V. *Chem. Phys. Lett.* **2007**, *444*, 205–208.
- (18) Damme, S. V.; Bultinck, P.; Fias, S. *J. Chem. Theory Comput.* **2009**, *5*, 334–340.
- (19) Bultinck, P.; Cooper, D. L.; Neck, D. V. *Phys. Chem. Chem. Phys.* **2009**, *11*, 3424–3429.
- (20) Lillestolen, T. C.; Wheatley, R. J. *J. Chem. Phys.* **2009**, *131*, 144101–1–144101–6.
- (21) Parr, R. G.; Ayers, P. W.; Nalewajski, R. F. *J. Phys. Chem. A* **2005**, *109*, 3957–3959.
- (22) Warburton, P. L.; Wang, J. L.; Mezey, P. G. *J. Chem. Theory Comput.* **2008**, *4*, 1627–1636.
- (23) Bader, R. F. W.; Matta, C. F. *J. Phys. Chem. A* **2004**, *108*, 8385–8394.
- (24) Rodrigues, E. F. F.; de Sá, E. L.; Haiduke, R. L. A. *Int. J. Quantum Chem.* **2008**, *108*, 2417–2427.
- (25) Bader, R. F. W.; Larouche, A.; Gatti, C.; Carroll, M. T.; MacDougall, P. J.; Wiberg, K. B. *J. Phys. Chem. A* **1988**, *87*, 1142–1152.
- (26) Poirier, R. A.; Hollett, J. W. *MUNgauss (Fortran 90 version)*; Chemistry Department, Memorial University: St. John's, NL A1B 3X7, 2010. With contributions from S. D. Bungay, F. Colonna, A. El-Sherbiny, T. Gosse, D. Keefe, A. Kelly, C. C. Pye, D. Reid, M. Shaw, M. Staveley, Y. Wang, P. L. Warburton, J. Xidos.
- (27) Becke, A. D. *J. Chem. Phys.* **1988**, *88*, 2547–2553.
- (28) Slater, J. C. *Phys. Rev.* **1930**, *36*, 57–64.